AGU PUBLICATIONS

Space Weather

RESEARCH ARTICLE
10.1002/2016SW001533

Key Points:
- Integral fluxes derived from coarse spectra using correct effective energies are accurate
- GOES and STEREO spectra agree well during the December 2006 solar proton event
- Current GOES integral fluxes are too high by up to a factor of 3

Correspondence to:
J. V. Rodriguez,
juan.rodriguez@noaa.gov

Citation:
Rodriguez, J. V., I. Sandberg, R. A. Mewaldt, I. A. Daglis, and P. Jiggens (2017), Validation of the effect of cross-calibrated GOES solar proton effective energies on derived integral fluxes by comparison with STEREO observations, *Space Weather*, *15*, 290–309, doi:10.1002/2016SW001533.

Received 14 SEP 2016
Accepted 8 DEC 2016
Accepted article online 13 DEC 2016
Published online 2 FEB 2017

©2016. The Authors.
This is an open access article under the terms of the Creative Commons Attribution-NonCommercial-NoDerivs License, which permits use and distribution in any medium, provided the original work is properly cited, the use is non-commercial and no modifications or adaptations are made.

Validation of the effect of cross-calibrated GOES solar proton effective energies on derived integral fluxes by comparison with STEREO observations

J. V. Rodriguez[1,2], I. Sandberg[3,4], R. A. Mewaldt[5], I. A. Daglis[4,3], and P. Jiggens[6]

[1]Cooperative Institute for Research in Environmental Sciences, University of Colorado Boulder, Boulder, Colorado, USA, [2]National Centers for Environmental Information, National Oceanic and Atmospheric Administration, Boulder, Colorado, USA, [3]Institute of Accelerating Systems and Applications, Athens, Greece, [4]Department of Physics, National and Kapodistrian University of Athens, Athens, Greece, [5]California Institute of Technology, Pasadena, California, USA, [6]European Research and Technology Centre, European Space Agency, Noordwijk, Netherlands

Abstract The derivation of integral fluxes from instrument coincidence rates requires accurate knowledge of their effective energies. Recent cross calibrations of GOES with the high-energy-resolution Interplanetary Monitoring Platform (IMP) 8 Goddard Medium Energy Experiment (GME) (Sandberg et al., *Geophys. Res. Lett*, *41*, 4435, 2014a) gave significantly lower effective energies than those currently used by the NOAA Space Weather Prediction Center to calculate solar proton integral fluxes from GOES rates. This implies systematically lower integral fluxes than currently produced. This paper quantifies the differences between the current and the cross-calibrated GOES integral fluxes and validates the latter. Care is taken to rule out the spectral resolution of the measurements or different integration algorithms as major contributors to differences in the magnitudes of the derived integral fluxes. The lower effective energies are validated by comparison with the independent, high-resolution observations by the STEREO Low-Energy Telescope (LET) and High-Energy Telescope (HET) during the December 2006 solar proton events. The current GOES product is similar to the >10 MeV integral fluxes recalculated by using the *Sandberg et al.* [2014a] effective energies but is substantially greater at higher energies. (The median ratios of the current to the recalculated fluxes are 1.1 at >10 MeV, 1.7 at >30 MeV, 2.1 at >60 MeV, and 2.9 at >100 MeV.) By virtue of this validation, the cross-calibrated GOES integral fluxes should be considered more accurate than the current NOAA product. The results of this study also demonstrate good consistency between the two long-term IMP 8 GME and STEREO LET and HET solar proton data sets.

1. Introduction

Since the beginning of the space age, the radiation hazard from solar proton events (SPEs) has been characterized in terms of their integral fluxes above selected threshold energies. For the purpose of calculating hazards to human space flight, *Webber et al.* [1963] characterized events observed between 1956 and 1962 in terms of their >10, >30, and >100 MeV integral fluences (time- and solid-angle-integrated fluxes, protons cm^{-2}) derived from ionospheric radio absorption and balloon- and satellite-borne particle measurements [see also *Malitson and Webber*, 1963]. The >30 and >100 MeV integral fluxes were used to calculate radiation dose to humans for nine spacecraft shielding configurations. The Solar Proton Monitoring Experiment (SPME), measuring >10, >30, and >60 MeV proton integral fluxes, was designed as a "simple and easily reproducible detector system to form the basis of an operational monitoring program" [*Bostrom et al.*, 1968; *Kohl*, 1968]. SPME flew on several missions in the late 1960s and early 1970s, including the Interplanetary Monitoring Platform (IMP) F, G, and I missions and polar-orbiting NOAA satellites in the Improved TIROS Operational System series. Hourly integral fluxes produced by this operational monitoring program from May 1967 to May 1973 were initially published in the NOAA National Geophysical Data Center's Solar-Geophysical Data reports. The IMP SPME data, along with other instruments' observations interpolated to the SPME energies, were used to construct a series of interplanetary proton models for use in mission design [*King*, 1974; *Stassinopoulos and King*, 1974; *Armstrong et al.*, 1983; *Feynman et al.*, 1990, 1993]. In the earlier models [*King*, 1974; *Stassinopoulos and King*, 1974], the data were extrapolated to >100 MeV. The JPL 1991 model [*Feynman et al.*, 1993] supplemented the integral fluxes above the three SPME energies with >1 and >4 MeV integral fluxes.

Since 1976, the NOAA Space Weather Prediction Center (SWPC) has characterized large SPEs observed by the Geostationary Operational Environmental Satellites (GOES) in terms of their >10 MeV flux (protons $cm^{-2}\,sr^{-1}\,s^{-1}$), both the onset (at 10 protons $cm^{-2}\,sr^{-1}\,s^{-1}$) and peak flux. However, NOAA specified an Energetic Particle Sensor (EPS) for GOES with proton channels of finite energy width [*Grubb*, 1975], rather than physical channels that were semi-infinite in energy. Therefore, GOES proton integral fluxes are calculated from a combination of multiple EPS rates. The algorithm used on GOES 7–15 (R. Zwickl, unpublished note, 1989, hereafter referred to as Z89; see Appendix A for a description of this algorithm) calculates integral fluxes above a set of seven threshold energies (1, 5, 10, 30, 50, 60, and 100 MeV). The >10, >50, and >100 MeV solar proton integral fluxes are plotted in real time at http://www.swpc.noaa.gov/. SWPC issues near-real-time operational warnings and alerts for robotic and human space flight based on the >10 MeV fluxes, while the >100 MeV integral fluxes support SWPC's warnings and alerts for suborbital human flights, including commercial transpolar airline routes (issued when the >100 MeV flux exceeds 1 proton $cm^{-2}\,sr^{-1}\,s^{-1}$). GOES integral proton fluxes interpolated to $E > 2.2$ MeV and $E > 5.2$ MeV serve as inputs to operational predictions of *D* region absorption of high-frequency and very high-frequency radio waves in the polar regions [*Sauer and Wilkinson*, 2008]. The Aerospace Corporation's Spacecraft Environmental Anomalies Expert System—Real Time (SEAESRT) for geosynchronous orbit, in operation at SWPC, uses the GOES >30 MeV protons to indicate the likelihood of single-event effects and the >5 MeV protons to indicate the risk of solar array power loss due to radiation dose increases [*O'Brien*, 2009].

The GOES EPS proton channels are broad in energy and relatively few. In converting rates from a finite but broad energy channel to differential fluxes, one faces the problem of deriving the effective energy of the differential fluxes. The effective energy can be derived from an inversion of the measurement integral. The Z89 algorithm uses fixed energies derived from the laboratory calibrations. Using the same band edges, *Kress et al*. [2013] solved for the effective energy iteratively assuming a power law spectrum. The first version of the Solar Energetic Particle Environment Modeling (SEPEM) Reference Data Set (RDS) was created based on a simple cross calibration of fluxes after interpolating the GOES EPS and IMP 8 Goddard Medium Energy Experiment (GME) instruments to the same energies assuming that the geometric mean value of the bin limits was an appropriate proxy for the effective energy in both cases [*Crosby et al*., 2015]. *Sandberg et al*. [2014a, hereafter referred to as S14] derived effective energies for six of the EPS channels through cross calibration with the high-energy-resolution Goddard Medium Energy Experiment (GME) on IMP 8. The resulting data set merged from all the GOES, and the earlier Synchronous Meteorological Satellite data now form version 2 of the SEPEM RDS. With these parallel developments, the question as to which set of EPS effective energies is more accurate has remained open.

An opportunity to address this question arose shortly after the launch of STEREO, during the December 2006 SPEs, when STEREO A and B were closely separated in highly elliptical Earth orbit. This opportunity has already been used to cross compare STEREO with several near-Earth differential proton flux observations [*Mewaldt et al*., 2007, 2015; *Lario et al*., 2013; *Richardson et al*., 2014]. (The last data from IMP 8 GME were recorded on 07 October 2006.) Since the STEREO and IMP 8 GME observations have comparable energy resolution, the December 2006 events provide a unique opportunity to validate the S14 effective energies for GOES. This paper addresses three major questions: (1) how well do integral fluxes calculated from high-resolution IMP 8 GME spectra agree with those calculated from low-resolution, cross-calibrated GOES spectra, (2) how well do the STEREO differential energy spectra agree with the cross-calibrated GOES spectra during the December 2006 events, and (3) how does the use of the S14 effective energies affect the derived GOES integral fluxes? The answers to the first two questions serve as necessary validation prior to drawing conclusions from the answers to the third. We find that the use of the S14 effective energies results in good agreement between the IMP 8 and GOES integral fluxes, and between the STEREO and GOES differential and integral fluxes. Moreover, the resulting integral fluxes are significantly lower than those currently derived by NOAA in real time from the GOES observations.

2. Data

The GOES fluxes used in this study are from the EPS on GOES 5, 7, 8, and 11. The EPS detector design is the same on GOES 4 through 15, apart from a reduction in the geometrical factor of the Dome D3 detector (which produces proton channel P4) starting with GOES 8 [*Onsager et al*., 1996]. *Rodriguez et al*. [2014] have shown

Table 1. STEREO LET and HET Proton Energy Bins Used in This Paper[a]

LET Proton Bins			HET Proton Bins		
Number	E_l (MeV)	E_u (MeV)	Number	E_l (MeV)	E_u (MeV)
1	1.8	3.6	1	13.6	15.1
2	3.6	4.0	2	14.9	17.1
3	4.0	4.5	3	17.0	19.3
4	4.5	5.0	4	20.8	23.8
5	5.0	6.0	5	23.8	26.4
6	6.0	8.0	6	26.3	29.7
7	8.0	10.0	7	29.5	33.4
8	10.0	13.6	8	33.4	35.8
			9	35.5	40.5
			10	40.0	60.0
			11	60.0	100.0

[a]Bin energies are the same for STEREO A and B. LET bin 8 is calculated by power law extrapolation from bins 6 and 7 and used in place of the 10–12 MeV physical bin, which has a spectrally dependent efficiency. LET-A bin 2 showed erratic noise of unknown origin during the December 2006 SPEs and therefore is excluded from the data.

that the relative responses of the GOES 8 through 15 EPS models agree to within ±20%. In the present study, only the effective energies are varied, not the fluxes produced by NOAA. The EPS P1 channel is not considered in this study because in addition to solar protons, it observes trapped magnetospheric protons not observed by IMP 8 or STEREO [*Green et al*., 2004].

The IMP 8 GME consisted of three particle telescopes, two of which are relevant to the present work, the Low Energy Detector (LED) and the Medium Energy Detector (MED) [*McGuire et al*., 1986]. Together, the LED and MED measured protons in 24 logarithmically spaced channels between 4.2 and 485 MeV. S14 have used this data set to derive effective energies for the six GOES EPS channels in this energy range, after correcting the channels affected by the gradual failure of the LED active anticoincidence circuit between 1984 and 1990.

The STEREO In-situ Measurements of Particles and CME Transients investigation comprises four instruments, data from two of which are used in this paper: the Low-Energy Telescope (LET) [*Mewaldt et al*., 2008] and the High-Energy Telescope (HET) [*von Rosenvinge et al*., 2008]. The LET and HET on STEREO A and B have the same design. LET has two segmented fan fields of view (FOV), 133° in the ecliptic by ±14.5° out of the ecliptic, that look along the nominal Parker spiral direction, one sunward and one antisunward. HET has a single conical (55° full-angle) FOV directed westward of the Sun along the nominal Parker spiral. LET measures the proton spectrum in eight channels between 1.8 and 13.6 MeV, while HET provides 11 proton channels between 13.6 and 100 MeV (the greatest effective energy being 76 MeV) (Table 1). (By comparison, IMP 8 GME had 18 channels between 4.2 and 100 MeV.) In this paper, the 10–12 MeV LET channel is not used due to its spectrally dependent efficiency (85–90%). Rather, it is replaced with a value in the 10–13.6 MeV gap between LET and HET extrapolated by using a power law fit to the 6–8 and 8–10 MeV LET channels. The channel energies are estimated as the energy where the flux is equal to the integral of the spectrum over the energy bin (using the actual spectral slope) divided by the width of the energy bin. This is equivalent to the iterative method used to calculate GOES effective energies discussed below. Galactic cosmic ray backgrounds are significant in the two highest-energy HET channels. They are removed by calculating the average uncorrected fluxes from December 1 through 12:00 UT on 5 December and from 25 to 31 December, and subtracting these averages from the observed fluxes.

All of the STEREO observations during the December 2006 events were taken during a single pair of closely spaced highly elliptical orbits (perigee on 12 December), ended by a lunar swing-by late on 15 December that sent the two spacecraft into their separate orbits [*von Rosenvinge et al*., 2009]. All STEREO data taken when either spacecraft was inside the magnetopause (0400–1700 UT) are omitted from the analysis. Moreover, the LET-A computer stopped operating during this radiation belt pass and was not restarted until the 2200 h on 15 December. STEREO-B was flying upside down during this period; therefore, the LET-B and HET-B look directions are centered perpendicular to the nominal Parker spiral direction at 1 AU, and therefore perpendicular to the LET-A and HET-A look directions [*Mewaldt et al*., 2009; *von Rosenvinge et al*., 2009]. The LET field of view about the ecliptic plane is effectively reduced when dynamic thresholds change in order to reduce dead-time at high flux levels [*Mewaldt et al*., 2008]. Dynamic thresholds changed several times during the December 2006 events, and these changes were accounted for in the processing. For this paper, the LET fluxes are omnidirectional averages of those detector combinations for which the dynamic thresholds have not been raised.

For comparisons between GOES and STEREO, solar wind dynamic pressure observations are taken from the OMNI data set [*King and Papitashvili*, 2005].

Table 2. GOES EPS Channel Energies Used in the December 2006 Calculations[a]

Channel	E_l (MeV)	E_{eff} (MeV)	E_{gm} (MeV)	E_u (MeV)
P1	0.6	[1.6]	1.6	4.2
P2	4.2	6.4	6.04	8.7
P3	8.7	12.5	11.2	14.5
P4	15.	20.8	25.7	44.
P5	39.	46.1	56.6	82.
P6	84.	104.	130.	200.
P7	110.	148.	234.	500.

[a]The lower and upper channel energies E_l and E_u are those used by the Z89 algorithm. The geometric mean of these energies, E_{gm}, is the starting point for the GOES-R iterative solution for the channel effective energy. E_{eff} are from *Sandberg et al.* [2014a] (S14) for GOES 11 except for P1.

3. Methods for Calculation of Integral Flux

In this paper, the GOES integral fluxes are calculated by using a piecewise power law to represent the differential number flux spectrum. The spectral pieces are defined by characteristic energies of the EPS channels and estimates of the differential number fluxes in these channels. The integral fluxes in each piece are calculated analytically, after which they are summed in order to estimate the total integral flux. (This method is used in section 5; a variant of this method is used in section 4.) The highest-energy segment involves extrapolation to some energy well above the effective energy of the highest-energy measurement. In the case of the December 2006 events, one set of integral fluxes is produced in real time by SWPC by using the Z89 algorithm. The other two sets are derived by using a simpler quadrature method, with different channel effective energies, one being derived from the Z89 set and the other from S14 (Table 2). The Z89 channel energies are derived from the proton beam calibrations of the GOES 4–6 engineering and flight models [*Panametrics*, 1979, 1980a]. The latter method is used to compare GOES and IMP 8 integral fluxes.

Since its introduction, the Z89 integral flux algorithm has been used by SWPC to calculate integral flux from the GOES EPS channel fluxes. This algorithm removes the slowly varying backgrounds, corrects for high-energy contamination of lower energy channels, and estimates the integral flux from the corrected channel fluxes. Its outputs include the corrected channel fluxes in units of differential number flux and the integral fluxes above a set of seven threshold energies. In this paper, we use the Z89 integral fluxes and corrected channel fluxes unaltered; the latter are the inputs to the GOES integral flux calculations in section 5. For details of the Z89 algorithm, please refer to the appendix.

With the S14 effective energies, the integral flux is calculated by using a simple quadrature method from EPS channel fluxes. A piecewise power law is defined by the observed differential fluxes and the fixed effective energies of S14. Assuming a power law, the differential number fluxes at adjacent effective energies are expressed as

$$\begin{aligned} j_i &= \alpha_i E_i^{-\gamma_i} \\ j_{i+1} &= \alpha_i E_{i+1}^{-\gamma_i} \end{aligned} \tag{1}$$

The integral flux between two effective energies is given by

$$J = \frac{\alpha_i}{-\gamma_i + 1}\left(E_{i+1}^{-\gamma_i+1} - E_i^{-\gamma_i+1}\right) \tag{2}$$

where the power law exponent is given by

$$\gamma_i = \ln\left(\frac{j_{i+1}}{j_i}\right) \Big/ \ln\left(\frac{E_i}{E_{i+1}}\right) \tag{3}$$

The minimum and maximum power law exponents and the default exponents used at background flux levels are the same as in the Z89 algorithm (Appendix A). Given that the threshold energy E_t lies within the lower and upper bounds E_l and E_u of one channel, the lowest energy contribution to the integral flux is calculated one of two ways. If the threshold energy is greater than the effective energy of channel i, the integral flux between the threshold energy and the effective energy of the next higher-energy channel ($i + 1$) is calculated by using a form of equation (2) with E_i replaced by E_t. If the threshold energy is less than the channel effective energy, the integral flux between the threshold energy and the effective energy of the channel in which it lies

is calculated by using a downward extrapolation of the power law defined by channels i and $i+1$. The intent of this step is to prevent the trapped proton fluxes at lower energies from affecting the >5 MeV integral fluxes. For EPS, the former condition holds for the >30 and >60 MeV integral fluxes, while the latter condition holds for the >1, >5, >10, and >100 MeV fluxes. In the case of the >50 MeV calculation, this depends on whether the S14 effective energy for GOES 11 P5 (46.1 MeV) or the geometric mean of the P5 edge energies (56.6 MeV) is used as the effective energy in the GOES-R algorithm (Table 2).

The iterative GOES-R method, developed for the new solar proton measurements on the next generation of NOAA geostationary weather satellites, is applied to EPS for comparison here because it is intermediate between the first two methods, combining the channel edge energies used by Z89 with the quadrature method used with the S14 energies. The piecewise power law exponents and channel effective energies are solved for iteratively, with the observed fluxes fixed. In this approach, the geometric means of the channel edge energies (Table 2) are used as the first guess for the channel effective energies. The energy E_i at which the differential channel flux is equal to the flux given by a power law spectrum is, for $\gamma \neq 0$ or $\gamma \neq 1$ [*Kress et al.*, 2013],

$$E_i = \left[\frac{(-\gamma+1)(E_u - E_l)}{\left(E_u^{-\gamma+1} - E_l^{-\gamma+1}\right)}\right]^{\frac{1}{\gamma}} \tag{4}$$

(Note that for $\gamma = 2$, this expression reduces to the geometric mean of E_l and E_u.) If $\gamma = 1$, then the expression is

$$E_i = \frac{(E_u - E_l)}{\ln\left(\frac{E_u}{E_l}\right)} \tag{5}$$

If $\gamma = 0$, then the differential flux is correct at all energies in the band, and the average channel energy can be used. The iteration on E_i proceeds until the change in E_i is less than 1%, with a maximum of 20 iterations. Again, the minimum and maximum power law exponents and the default exponents used at background flux levels are the same as in the Z89 algorithm (see Appendix A).

The fluxes calculated by using different methods or from different satellites are compared by calculating the quartiles (Q_1, Q_2, and Q_3) of the flux ratios [*Morley et al.*, 2016] at fixed energies:

$$n\text{th quartile} = Q_n\left(\frac{x_A}{x_B}\right) \tag{6}$$

where $n = 1$, 2, or 3 corresponding to 25%, 50%, and 75%; x is the differential flux at some energy or the integral flux above some energy; and "A" and "B" indicate different satellites or different products of the same inputs.

In order to distinguish the impact of very noisy samples on this estimate, the quartiles are calculated for fluxes above certain levels as well as for all fluxes. For the >10 MeV and >100 MeV integral fluxes, the threshold flux levels used by SWPC operations to issue SPE alerts are used (10 and 1 $cm^{-2}\,s^{-1}\,sr^{-1}$, respectively). For the >30 and >60 MeV integral fluxes, levels are used (5 and 3 $cm^{-2}\,s^{-1}\,sr^{-1}$, respectively) that are 10 times those planned to be used to identify the onset of large SPEs (before alerts are issued) observed by GOES-R at these energies.

4. Comparison of IMP 8 and GOES Integral Fluxes, 1984–2001

The S14 effective energies correspond to the values one may attribute to the differential proton flux measurements of GOES EPS in order to obtain the best agreement with IMP 8 GME measurements. It is evident that the use of the effective energies for GOES differential channels will affect the integral flux calculations as well. However, before investigating the consequences of using the effective energy values in the integration schemes applied to GOES EPS data, it is crucial to verify that the effective integral GOES fluxes are in agreement with IMP 8 GME. It should be noted that this is not a priori ensured given the restricted spectral resolution provided by six EPS channels in comparison with the dense energy binning provided by the 24 differential channels of GME in the same energy range.

For the calculation of the integral fluxes we apply a simple numerical integration scheme which uses only the logarithmic centered values of the IMP 8 GME nominal energy proton bins and the effective energy values for the GOES channels (S14). The GOES and GME differential proton fluxes are initially re-binned (using a piecewise power law interpolation scheme) to the same dense proton energy grid of 100 logarithmically equally distanced

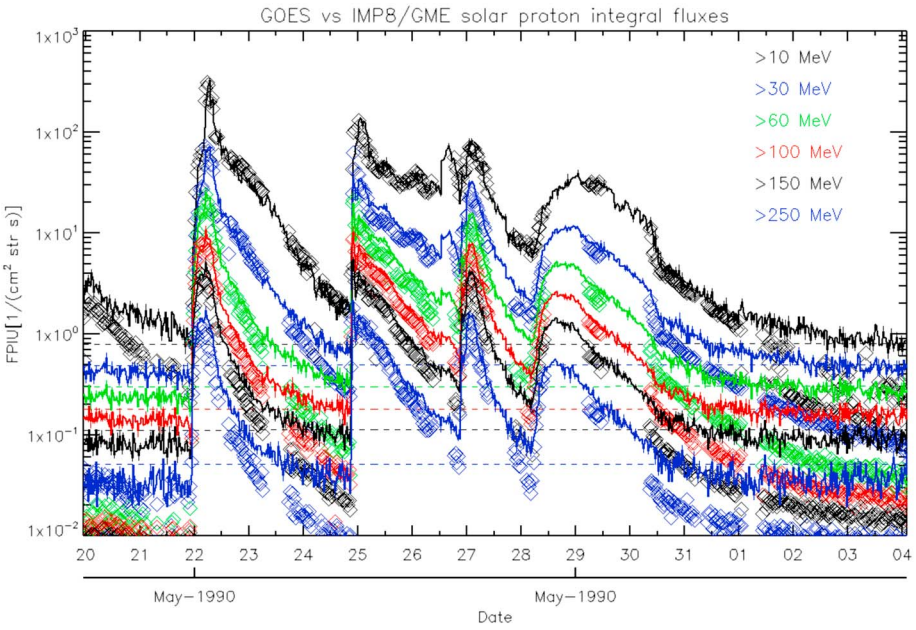

Figure 1. Time series of GOES 7 EPS and IMP 8 GME integral proton fluxes for the series of large SPEs during late May 1990, calculated by using the integration method described in section 4. The EPS integral fluxes are represented by continuous lines, while the GME integral fluxes are represented by discrete symbols. The dashed lines represent the upper limit of the background fluctuations of GOES integral fluxes calculated during these events. (FPIU = directional integral proton flux).

bins within the energy range of 5–500 MeV. Then, they are integrated for energies above 10, 30, 60, 100, 150, and 250 MeV. GOES integral fluxes calculated by using this method and the integration method described in section 3 agree well when a common set of channel effective energies is used [*Sandberg et al.*, 2014b].

Before proceeding to the comparisons, it is crucial to be aware of the uncertainties arising during the integration procedure. The integration of IMP 8 GME flux data set suffers from the frequent presence of NaN values attributed to the postprocessing during the data cleaning. Apart from the cases where all the spectral points are NaNs, 54% of the spectra have no NaNs, 29% have 1–4 NaNs, and 17% have more than four NaNs. Since spectral points with NaNs are omitted from the integral, there is some underestimation when NaNs are present. However, since the integrals are dominated by the flux just above the threshold energies, and NaNs at these energies result in NaNs for the affected integral flux, this has a small impact on the overall comparison. Of broader concern for the calculation of GOES integral fluxes, the piecewise power law approximation might be inaccurate due to the sparse binning of GOES effective energy values, while the enhanced background levels (due to a combination of instrument noise and galactic cosmic rays) for the high-energy differential flux series might lead to overestimated integral values.

In Figure 1, as an example, we present the resulting GOES 7 and IMP 8 integral flux series calculated for the series of large SPEs that took place during late May 1990. We have selected this series due to the relatively large number of finite values in the IMP 8 GME cleaned data set. The integral fluxes correspond to threshold energies of 10, 30, 60, 100, 150, and 250 MeV. It is evident that the profiles of the effective integral GOES fluxes at the selected energies are in very good agreement with the corresponding IMP 8 values. Differences start to appear when the GOES integral fluxes approach the corresponding background levels (the upper limits of which are indicated by dashed lines).

For the comparison between GOES and IMP 8 integral proton fluxes, we consider their simultaneous measurements between 01 January 1984 and 25 October 2001, the period used by S14 in their cross calibration (312,413 points). In order to reduce the differences attributed to the extrapolation of the differential fluxes to energies far above their energy range (i.e., up to 500 MeV), we subtract the 250–500 MeV contribution from the integrals. We present in Figure 2 two-dimensional histograms of the scatter between IMP 8 GME and effective GOES integral fluxes within the 10–250, 30–250, 60–250, and 100–250 MeV energy ranges. The horizontal and perpendicular dashed lines correspond to predefined integral flux values of [10, 5, 3, 1] $cm^{-2}\,s^{-1}\,sr^{-1}$, the operational alert

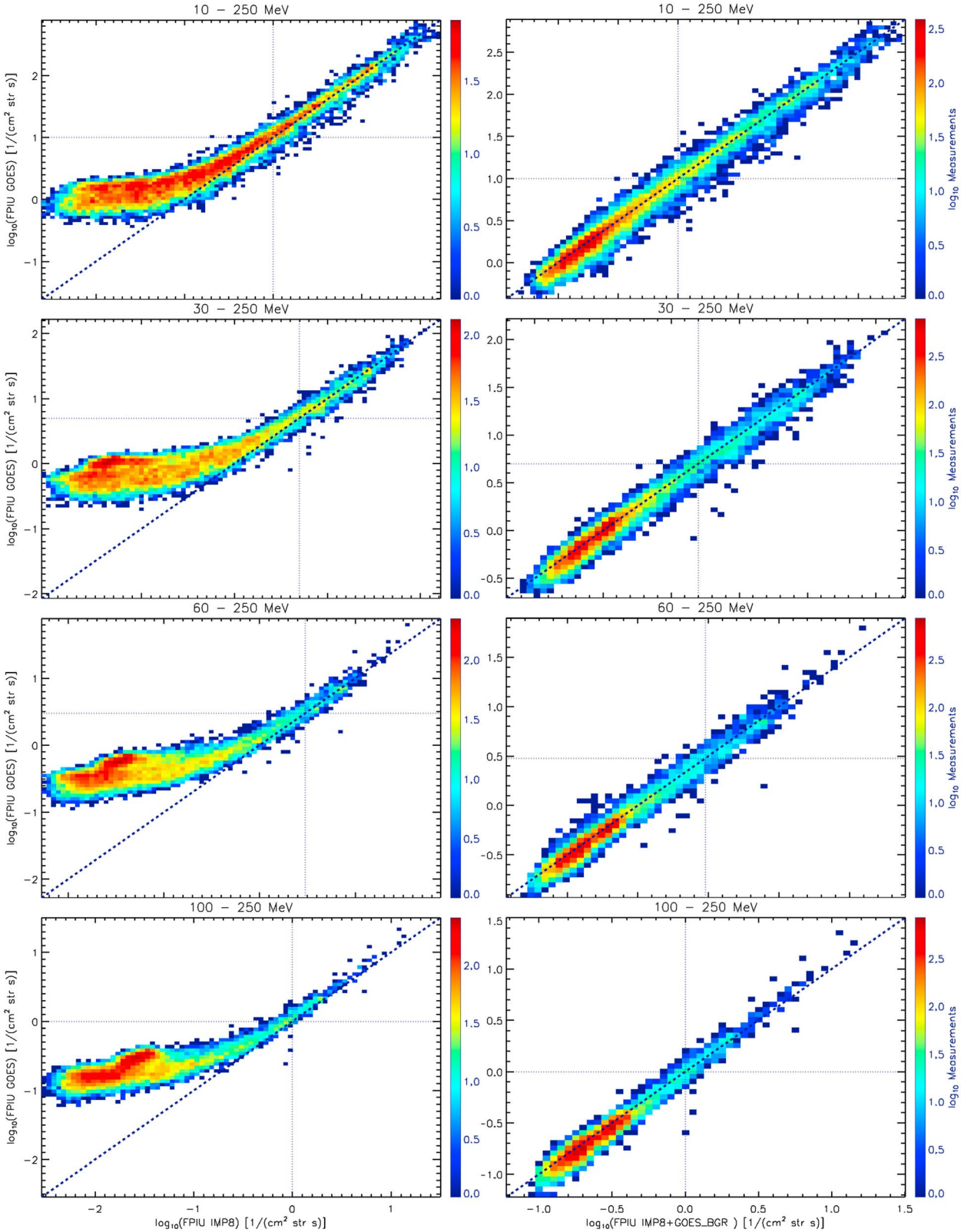

Figure 2. (left column) Two-dimensional histograms (density plots) of effective GOES and IMP 8 GME integral fluxes for the period 01 January 1984 to 26 October 2001 in four energy ranges (10–250 MeV, 30–250 MeV, 60–250 MeV, and 100–250 MeV). (right column) The plots correspond to IMP 8 GME integral fluxes with a background level artificially introduced that is equal to that of GOES EPS, as described in the text. For reference, $y = x$ curves are provided. The horizontal and perpendicular dashed lines correspond to the operational alert levels defined at the end of section 3.

Table 3. Quartiles of the Ratios of Proton Integral Fluxes (Equation (6)) Calculated From IMP 8 and From Cross-Calibrated GOES Data During 01 January 1984 to 26 October 2001[a]

	Ratios of IMP 8 to GOES Integral Fluxes				
Energy (MeV)	10–250	30–250	60–250	100–250	150–250
First quartile (Q_1)	0.942	0.959	0.984	1.008	1.002
Median (Q_2)	1.052	1.045	1.059	1.089	1.112
Third quartile (Q_3)	1.194	1.151	1.143	1.180	1.245

[a]The ratios here are of the IMP 8 fluxes to the GOES fluxes, with the GOES backgrounds added to the IMP 8 fluxes as described in the text.

levels defined at the end of section 3. As can be seen in Figure 2 (left column), significant deviations appear for intensities lower than the integral flux thresholds and close to GOES EPS background levels. In order to verify that these deviations are attributed exclusively to the background, we eliminate the contributions attributed to the different background levels of the derived fluxes. In order to do this, we calculate the varying background levels of GOES integral fluxes *BGR_GOES(E)* and add them to IMP 8 GME data. This is well justified given the fact that $BGR\_GOES(E) \gg BGR\_IMP8(E)$. The resulting integral fluxes can be considered as a virtual data set with calibration and energy resolution identical to IMP 8 GME and (enhanced) background levels identical to that of GOES EPS. Comparisons of this virtual data set with effective GOES integral fluxes are presented in Figure 2 (right column). The resulting two-dimensional histograms are well organized along the $y = x$ line, demonstrating that the systematic differences between the GOES and IMP 8 integral fluxes are dominated by the backgrounds in the former.

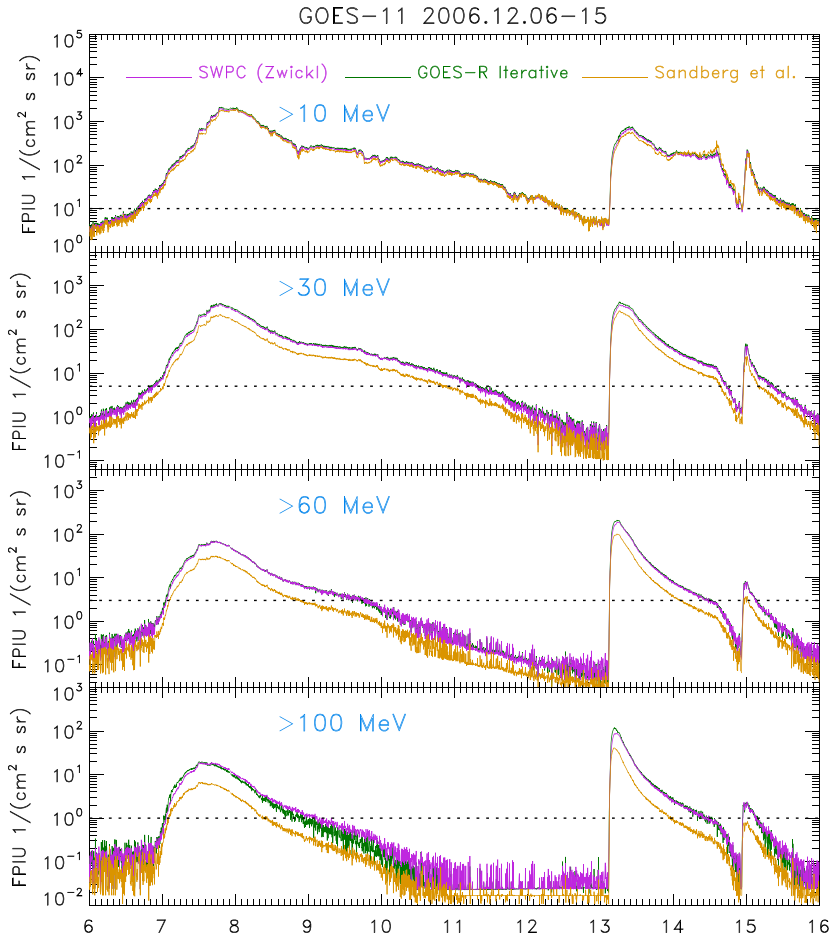

Figure 3. Comparison of integral fluxes above four energies during the December 2006 SPEs, calculated from GOES channel fluxes using three methods: SWPC's operational product (Z89, purple), the GOES-R algorithm with iteratively determined effective energies (green), and the same quadrature method as GOES-R, but with the fixed effective energies of S14 (goldenrod). As plotted, the SWPC result generally lies atop the GOES-R result at the three lower energies. The horizontal dotted lines indicate the flux thresholds used in the quartile determinations (Table 4).

Table 4. Quartiles of the Ratios of GOES 11 Proton Integral Fluxes (Equation (6)) During the December 2006 SPEs Calculated Using the GOES-R and S14 Methods and the Baseline Z89 Method (Figure 3)[a]

			Energy (MeV)			
Flux Ratios	Flux Range	Q_n	>10	>30	>60	>100
Z89/GOES-R	above thresholds	Q_1	0.927	0.918	0.945	0.917
		Q_2	0.940	0.932	0.968	0.983
		Q_3	0.953	0.945	0.990	1.170
	all	Q_1	0.927	0.906	0.932	0.946
		Q_2	0.941	0.930	0.964	1.042
		Q_3	0.954	0.946	1.002	1.488
Z89/S14	above thresholds	Q_1	1.029	1.667	2.053	2.650
		Q_2	1.095	1.735	2.132	2.871
		Q_3	1.166	1.758	2.250	3.176
	all	Q_1	1.020	1.668	2.033	2.013
		Q_2	1.091	1.732	2.147	2.872
		Q_3	1.162	1.768	2.296	3.507

[a]The flux thresholds are 10, 5, 3, and 1 $cm^{-2}\,s^{-1}\,sr^{-1}$ for the >10, >30, >60, and >100 MeV fluxes, respectively. Q_1, Q_2, and Q_3 correspond to the 25th, 50th and 75th percentiles.

In order to quantify the residual differences between the IMP 8 GME and effective GOES integral fluxes, we have calculated the median and first and third quartiles of the ratios of the GME fluxes (with the GOES backgrounds added) to the GOES fluxes (equation (6)). The results (Table 3) quantify the good agreement between the IMP 8 and cross-calibrated GOES integral fluxes that is apparent in the two-dimensional histograms. This result validates the estimation of integral fluxes by using the spectrally sparse GOES channel fluxes (with the backgrounds removed) assigned to the S14 effective energies to define a piecewise power law spectrum. This is particularly important for SPEs after the cessation of the high-resolution IMP 8 observations, for which we must rely on the GOES observations.

5. Comparison of GOES and STEREO Proton Fluxes During the December 2006 SPEs

5.1. Comparison of GOES Integral Fluxes Calculated Using Different Methods

Solar proton integral fluxes (>10, >30, >60, and >100 MeV) calculated by using the Z89 algorithm, the iterative GOES-R algorithm, and the S14 effective energies are shown in Figure 3 for 06–15 December 2006. The integral fluxes produced by the Z89 and GOES-R algorithms are similar; differences are difficult to discern visually, apart from some divergences at >100 MeV. The integral fluxes calculated by using the S14 effective energies are substantially lower at the higher energies, with the difference increasing with energy. The quartiles of the ratios of the Z89 to the GOES-R or S14 fluxes are summarized in Table 4, both for the complete time series and for those periods in which the Z89 fluxes were above the operational flux thresholds given earlier. The medians (Q_2) are similar in general between the two cases. The exception to this is the comparison between GOES-R and Z89 at >100 MeV, in which the median ratio for all flux levels is somewhat greater than the median for fluxes above the thresholds. The median ratios of the Z89 to GOES-R fluxes are reasonably close to unity, the largest deviation from unity being 0.932 at >30 MeV. The median ratios of the Z89 to S14 fluxes above the operational thresholds are 1.10 and 2.87 at >10 MeV and >100 MeV, the integral fluxes based upon which SWPC issues Solar Radiation Storm alerts, and 1.74 at >30 MeV, used in the SEAESRT model. These ratios indicate substantial systematic differences at the higher energies. Since the distinct GOES-R and Z89 algorithms produce integral fluxes that agree well using the same channel energies, the difference between the S14 (using the GOES-R integration method without iterating on the effective energies) and Z89 fluxes is dominated by the difference in effective energies. The next two sections therefore investigate whether the S14 or Z89 effective energies agree better with an independent data set, the STEREO LET and HET measurements.

5.2. Cross Comparison of GOES and STEREO Differential Fluxes

Prior to comparing GOES and STEREO integral fluxes, a comparison of differential fluxes is needed in order to understand sources of differences. Figure 4 shows two examples of GOES 11, STEREO A, and STEREO B spectra for low and high P_{dyn}. The GOES 11 spectra are plotted at the S14 effective energies and at the channel mean energies used by the Z89 algorithm. As noted previously, the agreement between STEREO A and B

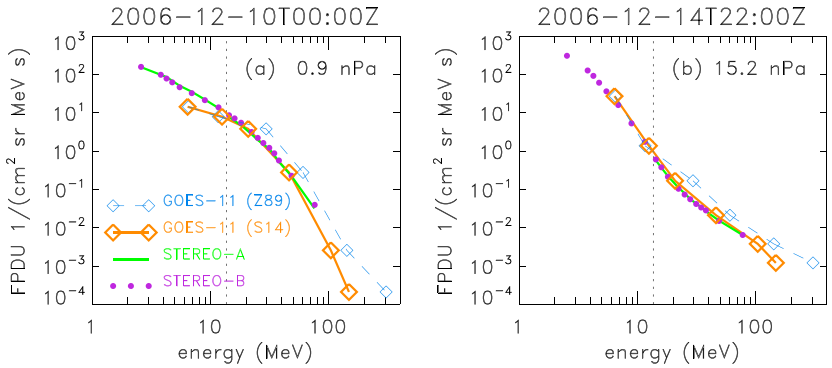

Figure 4. Two examples of GOES and STEREO spectra during periods of low and high solar wind dynamic pressure, (a) 10 December 2006, 0000–0100 UT, when the hourly P_{dyn} was 0.9 nPa, and (b) 14 December 2006, 2200–2300 UT, when the hourly P_{dyn} was 15.2 nPa. The STEREO A spectra are represented by a green line. The STEREO B spectra are represented by purple dots. The GOES spectra are plotted as a solid orange line against the S14 effective energies and as a dashed blue line against the Z89 effective energies, with diamonds indicating the data points. The vertical dotted line is at 13.6 MeV, separating the LET and HET spectra. No LET-A data were available in the second case. (FPDU = directional differential proton flux).

measurements is very good [*Mewaldt et al.*, 2015]. For the case with P_{dyn} = 0.9 nPa, the GOES fluxes are lower than the STEREO fluxes below ~20 MeV, during an undulation in the GOES fluxes due to enhanced geomagnetic cutoffs in the westward look direction of the GOES 11 EPS [*Rodriguez et al.*, 2010; *Rodriguez*, 2012; *Kress et al.*, 2013]. This effect is not present in the second case for which P_{dyn} = 15.2 nPa. Above ~20 MeV in both cases, the GOES spectra plotted at the Z89 energies are enhanced relative to the GOES spectra plotted at the S14 energies as well as the STEREO spectra. These two spectra indicate that the GOES spectra at the S14 energies derived from cross calibrations with IMP 8 GME agree much better with the STEREO spectra. The following analysis quantifies this apparent agreement over the entire period of interest (06–15 December 2006).

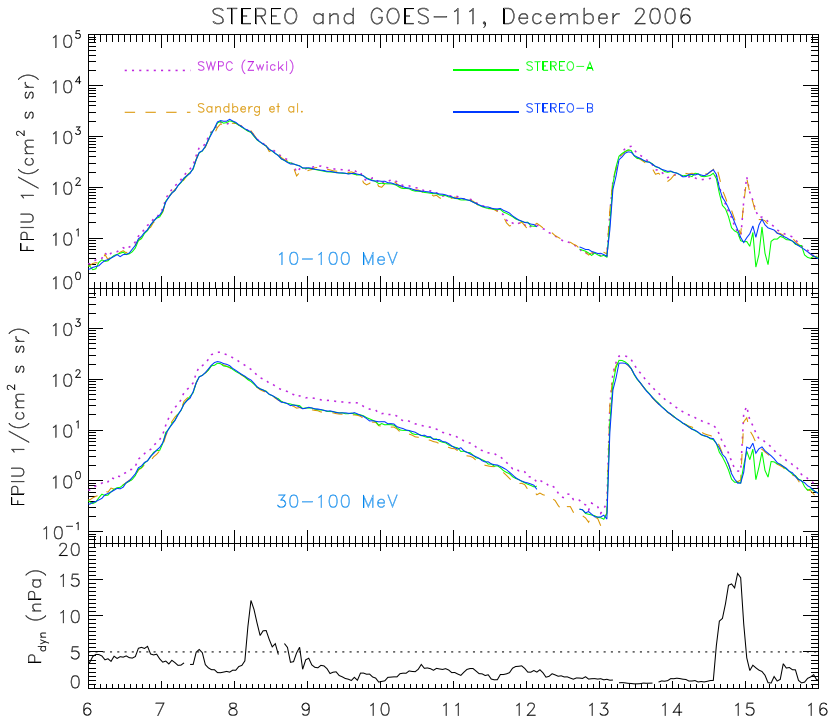

Figure 5. Comparison of (top) 10–100 MeV and (middle) 30–100 MeV integral fluxes observed by STEREO and GOES 11 during the December 2006 SPEs. The GOES 11 fluxes are calculated by using the Z89 algorithm and the S14 effective energies. (bottom) The solar wind dynamic pressure (P_{dyn}) from the OMNI data set. All data here are 1 h averages.

Table 5. Quartiles of the Ratios of STEREO to GOES 11 Differential Fluxes (Equation (6)) During the December 2006 SPEs, for all P_{dyn} and for $P_{dyn} \geq 5$ nPa

			Energy (MeV)					
Flux Ratios	P_{dyn} range	Q_n	6.4 (P2)	12.5 (P3)	20.8 (P4)	25.7 (P4)	46.1 (P5)	76
STEREO A/GOES 11 S14	all	Q_1	0.981	0.953	0.811	0.428	0.915	1.144
		Q_2	1.182	1.021	0.851	0.458	0.958	1.391
		Q_3	1.566	1.145	0.895	0.519	0.987	1.686
	≥5 nPa	Q_1	1.010	0.956	0.746	0.366	0.887	1.151
		Q_2	1.096	0.985	0.819	0.428	0.931	1.396
		Q_3	1.202	1.026	0.829	0.450	0.964	1.514
STEREO B/GOES 11 S14	all	Q_1	0.897	0.943	0.841	0.436	0.854	1.325
		Q_2	1.101	1.012	0.890	0.467	0.902	1.637
		Q_3	1.525	1.158	0.952	0.518	0.950	1.945
	≥5 nPa	Q_1	0.793	0.854	0.816	0.407	0.852	1.457
		Q_2	0.969	0.969	0.854	0.437	0.895	1.648
		Q_3	1.055	1.008	0.887	0.452	0.923	1.748

The cross comparison here is performed under the conditions that the solar proton fluxes are approximately homogeneous and isotropic between GOES and STEREO, with the exception of the effect of geomagnetic cutoffs at GOES. Therefore, the following periods are excluded from the quantitative comparison: 0400–1659 UT on 12 December, when one or both of the STEREO satellites were inside the magnetosphere, in order to avoid contamination from the radiation belts; 0300–0859 UT on 13 December, when the lower energy GOES channels were severely contaminated by the hard proton spectra during ground level enhancement (GLE) 70 (0250 UT onset [e.g., *Matthiä et al*., 2009]); and after the passage of the shock late (2300 UT on 14 December through 0959 UT on 15 December), when the fluxes were strongly inhomogeneous (between GOES 11 and STEREO) and anisotropic (at STEREO, see Figure 5) [*Mulligan et al*., 2007; *von Rosenvinge et al*., 2009]. This leaves 210 one-hour spectra to compare (151 for LET-A).

The quartiles for the ratios of the STEREO to the GOES spectra are determined at six energies as follows. The high-resolution STEREO spectra are interpolated to the GOES P2-P5 (6.4–46 MeV; Table 2) effective energies, and the GOES P5 and P6 fluxes are interpolated to the highest-energy STEREO HET energy (76 MeV). In addition, for comparison with the *Lario et al*. [2013] cross calibration between GOES P4 and HET, the STEREO spectra are interpolated to the geometric mean of the P4 edge energies (25.7 MeV) (Table 2). Piecewise power law interpolation is used. For this comparison of solar proton observations inside and outside the magnetosphere, the quartiles are also calculated for the subset of spectra for which solar wind dynamic pressure (P_{dyn}) is greater than or equal to 5 nPa (Figure 5). This is based on the recognition [*Rodriguez et al*., 2010, 2014; *Kress et al*., 2013] that geomagnetic cutoff effects increase as channel energy and P_{dyn} decrease.

The results are summarized in Table 5. The pattern of comparisons is similar between both STEREO A and B and GOES 11. The median ratios of the STEREO to GOES 11 fluxes indicate good agreement at the S14 energies for P2–P5 (6.4–46.1 MeV), ranging from 0.819 to 1.18. The median ratios are substantially larger for all P_{dyn} than for P_{dyn} above 5 nPa at all energies except 76 MeV. At the lower energies, this systematic difference may be due in part to suppressed geomagnetic cutoffs during the period of $P_{dyn} > 5$ nPa (relatively larger GOES fluxes resulting in a smaller ratio). When P4 is attributed to the geometric mean energy of 25.7 MeV, 4.9 MeV greater than the S14 energy, the medians decrease to 0.428–0.467. This is roughly consistent with the factor of 1.6 that *Lario et al*. [2013] used to reduce the P4 fluxes for comparison with HET, noting that their factor of 1.6 was derived over a shorter period (13–14 December) and that they did not give the energy to which the HET fluxes were interpolated.

At 76 MeV, the median ratios are larger than at the lower energies: 1.39 and 1.64 for STEREO A and B (1.40 and 1.65 for $P_{dyn} \geq 5$ nPa). These larger ratios could be due in part to the use of a single power law to interpolate the GOES fluxes over a 58 MeV range (P5 and P6). Although, throughout this period, the HET fluxes at 76 MeV lie both above and below the power law defined by P5 and P6, the lower quartiles are substantially greater than unity. Since GOES fluxes at these and higher energies are not significantly affected by geomagnetic cutoffs [*Rodriguez et al*., 2010], the differences may be dominated by time and directional variations in spectra that moreover depart from a single power law to some degree.

Table 6. Quartiles of the Ratios of STEREO to GOES 11 Integral Fluxes (Equation (6)) During the December 2006 SPEs, the Latter Calculated Using the Z89 and S14 Methods, Shown in Figure 5

		Energy (MeV)	
Flux Ratios	Q_n	10–100	30–100
STEREO A/STEREO-B	Q_1	0.947	0.951
	Q_2	0.976	0.985
	Q_3	0.995	1.015
STEREO A/GOES 11 Z89	Q_1	0.850	0.591
	Q_2	0.926	0.615
	Q_3	1.017	0.640
STEREO B/GOES 11 Z89	Q_1	0.874	0.602
	Q_2	0.948	0.624
	Q_3	1.071	0.660
STEREO A/GOES 11 S14	Q_1	0.927	0.987
	Q_2	0.975	1.044
	Q_3	1.061	1.113
STEREO B/GOES 11 S14	Q_1	0.948	1.002
	Q_2	1.002	1.060
	Q_3	1.094	1.152

5.3. Comparison of GOES and STEREO Integral Fluxes

To compare STEREO and GOES integral fluxes, we calculate 10–100 and 30–100 MeV fluxes so that no extrapolation of the STEREO fluxes is required. The STEREO integral fluxes are derived following the method of iterative determination of effective energies (section 3). The contribution between 76 and 100 MeV is determined by using the power law determined from the two highest-energy HET channels. When the LET-A instrument is off, the lowest-energy part of the 10–100 MeV integral is calculated from an extrapolation downward in energy of the power law defined by the two lowest-energy HET-A channels. The GOES 10–100 and 30–100 MeV integral fluxes are derived by simply subtracting the >100 MeV GOES fluxes from the >10 and >30 MeV fluxes. This has a small effect on the integral flux values, except during GLE70 (13 December 2006), where the difference is as much as 60%. The 10–100 and 30–100 MeV fluxes are plotted in Figure 5, and the flux ratio quartiles (equation (6)) are summarized in Table 6, calculated over the same valid intervals as the differential flux quartiles. The STEREO A and B integral fluxes agree very well, with median ratios of 0.976 (10–100 MeV) and 0.985 (30–100 MeV). The STEREO fluxes agree well with the S14 fluxes in both integral energy ranges, with median ratios of 0.975–1.06. As shown in section 4, the median ratios of 10–250 and 30–250 MeV integral fluxes calculated by using high-resolution (GME) and low-resolution (GOES) measurements are 1.052 and 1.045; therefore, any median ratios in this range between STEREO- and GOES-derived integral fluxes may be due largely to spectral resolution differences. While the STEREO and Z89 10–100 MeV fluxes agree reasonably well (median ratios of 0.926 and 0.948), at 30–100 MeV the median ratios are substantially smaller (0.615 and 0.624). When inverted (1.63 and 1.60), these are consistent with the median ratio of 1.7 of the GOES Z89 to the S14 > 30 MeV flux (Table 4). These comparisons between STEREO and GOES validate the S14 effective energies for the GOES channels and reveal large differences at >30 MeV and above with respect to the Z89 integral fluxes.

6. Discussion

The fortuitous nature of the cross calibrations of different generations of operational and science missions made possible by the December 2006 SPEs cannot be overemphasized. By virtue of their wide dynamic range during a period of large P_{dyn}, these events enabled the cross calibrations between the GOES 8–12 and 13–15 series of particle detectors [*Rodriguez et al.*, 2014]. However, it needs to be shown whether the December 2006 events provide a representative range of spectral variation and thereby a sound test of the S14 GOES effective energies. Histograms of the piecewise power law exponents (equation (3)) are shown in Figure 6 for groups of SPEs in solar cycles 23 and 24 with peak >10 MeV proton fluxes greater than 1000 protons/(cm^2 s sr), as determined by SWPC. The first of these events was in April 1998, and the last was in June 2015. These exponents were calculated by using the algorithm described in section 3 with the S14 effective energies. Histograms are plotted for the ensemble of all but the December 2006 events and separately for the December 2006 events. Power law exponents set to the default values for background values are omitted from the histograms, but the upper limit of 8 to the exponents set by the algorithm is evident in the histograms (see Appendix A for these default values). The histograms show that the exponents in the December 2006 events above 12.5 MeV (γ_{34} and higher) are systematically smaller (spectrally harder) on average than those in the larger ensemble. This may be due in part to the influence of GLE70; not all of the events in the ensemble corresponded to GLEs. Keeping in mind this bias toward harder spectra, the December 2006 events generally cover the same range of exponents as the larger ensemble and therefore can be considered spectrally

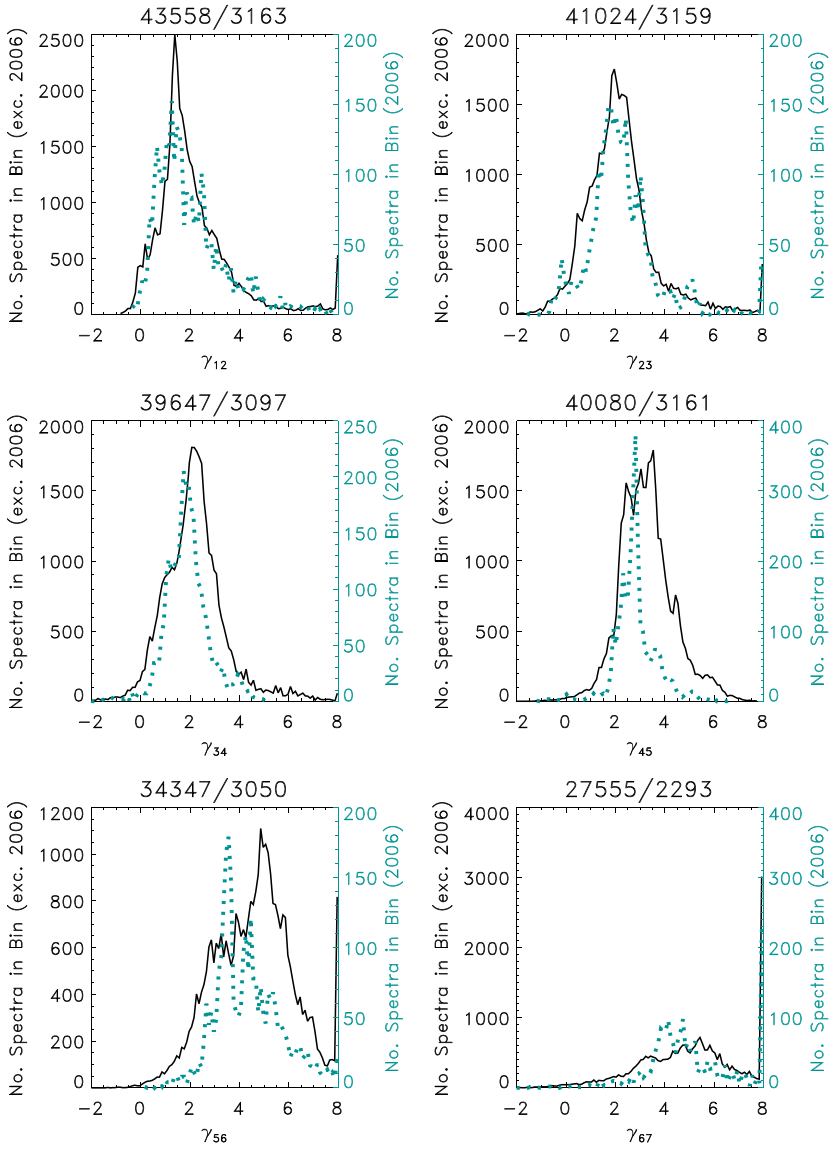

Figure 6. Histograms of piecewise-power law exponents ($\gamma_{i,i+1}$) for solar cycle 23 and 24 SPEs with peak >10 MeV proton flux greater than 1000 protons/(cm^2 s sr), calculated by using the algorithm described in section 3 with the S14 effective energies. The subscripts for the power law exponents (equation (3)) indicate the two GOES proton channels that define them (Table 2). The black solid curves are the histograms for all events except the December 2006 events (referred to the left-hand axis), while the green dotted curves are the histograms for just the December 2006 events (referred to the right-hand axis). The individual plot titles indicate the number of cases in the black curves (larger number) and green curves (smaller number). The bin size is one tenth of a power law exponent.

representative of large SPEs, at least in solar cycles 23 and 24. This does not diminish the value of future cross calibrations between GOES and higher-resolution proton measurements should the opportunity arise.

The cross comparisons performed here show that high-resolution STEREO and low-resolution GOES differential fluxes, and the integral fluxes derived from them, agree well when GOES effective energies derived from the S14 cross comparisons with the high-resolution IMP 8 GME are used. Also, the effective GOES integral fluxes are in excellent agreement with integral fluxes derived from the IMP 8 GME differential fluxes themselves. While the >10 MeV fluxes currently produced by NOAA using the Z89 algorithm agree well with the foregoing, the current product significantly overestimates the >30 MeV and higher-energy fluxes by factors of 1.7–2.9. Given this general overestimation of the GOES integral fluxes, cross calibrations that have treated the GOES integral fluxes as a "gold standard" [e.g., *Guild et al.*, 2009; *Ginet et al.*, 2013] should be

reevaluated. Any cross calibration that uses effective energies for the GOES differential fluxes should for consistency recalculate integral fluxes because the GOES integral fluxes are not independent measurements.

While some of the earliest integral flux observations came directly from physical channels with their own geometrical factors [*Bostrom et al.*, 1968], this has never been the case for GOES integral fluxes. Calculation of integral fluxes from channel fluxes may seem straightforward until one faces the question of which effective energies to use for the channels. The complexity in all the approaches followed in this paper stems from the determination or use of channel effective energies. Absent the opportunity to cross-calibrate with a higher-resolution measurement, future missions will have to rely on the derivation of effective energies from accurate simulations and measurements of the channel responses with respect to energy and angle.

The iterative GOES-R algorithm was developed with the goal of good agreement with the Z89 algorithm, given the same channel set and effective energies. The results here show that this goal was met. At the lowest energies (dominating the $>$10 MeV fluxes), where the relatively narrow channels come from the EPS telescope rather than one of the dome detectors, the output of the GOES-R algorithm agrees well with the S14 and STEREO results. The new GOES-R solar proton instrument is composed of three solid-state telescopes and provides improved spectral resolution with respect to the current EPS across the 1–500 MeV energy range, particularly above 100 MeV [*Dichter et al.*, 2015]. Therefore, the GOES-R integral flux algorithm, when used with accurate effective energies derived from simulations and measurements of the new instrument's channel responses, should provide accurate integral fluxes. Cross calibration of the new instrument with GOES 13–15 observations (using the S14 energies) during SPEs will provide an important "calibration transfer" from IMP 8 GME and STEREO LET and HET to GOES-R.

All of the methods used here are based on the assumption that a piecewise power law representation of the spectrum is adequate. While more advanced methods for retrieving a differential spectrum from finite-width channels are possible, the results here show that the median ratios of fluxes derived from high-resolution (IMP 8 GME, STEREO LET, and HET) spectra to those derived from low-resolution (GOES) spectra assuming a piecewise power law indicate good agreement if the effective energies are consistent. Although not a focus of this study, background subtraction is an essential though underappreciated step in any integral flux algorithm and is particularly important for accuracy at low flux levels. The current GOES measurements suffer from high backgrounds compared to GME and LET and HET. Therefore, prior to comparison, either GOES backgrounds must be added to the low-background measurement (as in section 4) or backgrounds must be removed from both sets (as in section 5).

It should be recognized that the STEREO LET and HET observations only provide a direct validation of the S14 GOES effective energies for channels P2–P5 (6.4–46 MeV). However, since the S14 method itself is certainly validated by this comparison, the P6 and P7 effective energies (104 and 148 MeV) are validated indirectly. The Payload for Antimatter Matter Exploration and Light-nuclei Astrophysics (PAMELA) mission is a good candidate for direct cross comparisons with GOES above 100 MeV, starting with the December 2006 SPEs [*Adriani et al.*, 2016].

Despite the stability in the GOES EPS solar proton channel design since GOES 4 (apart from P4), the geometry-energy factors used in the NOAA processing changed between GOES 7 and 8. These changes are reflected in the results of the S14 cross calibrations of the publicly available GOES data sets. Moreover, the single set of calibration parameters used for the GOES 8–15 processing differs from the definitive geometrical factors calculated by the instrument vendor [*Onsager et al.*, 1996, and references therein]. Although arguments have been made for reprocessing the data set using these definitive geometrical factors, the cross-calibrated S14 effective energies for the existing publicly available GOES data sets probably supersede the need for such reprocessing.

7. Conclusions

The conclusions of this work can be summarized as follows:

1. Integral fluxes calculated from high-energy-resolution IMP 8 GME spectra agree well with those calculated from low-resolution GOES spectra using the cross-calibrated effective energies of *Sandberg et al.* [2014a], with median ratios of IMP 8 to GOES fluxes ranging from 1.05 to 1.11. The period of this comparison was 01 January 1984 to 26 October 2001.
2. Evaluated at five interpolated energies, the STEREO differential energy spectra agree well with the cross-calibrated GOES spectra during the December 2006 events. At the *Sandberg et al.* [2014a] effective

energies, the median ratios of STEREO to GOES 11 flux (for all solar wind dynamic pressures) range from 0.85 to 1.18. At the highest STEREO HET energy (76 MeV), the median ratios are 1.39 and 1.64, due in part to the coarse spectral sampling at higher energies. This comparison constitutes a direct validation of the *Sandberg et al*. [2014a] effective energies from 6.4 to 46 MeV, and an indirect validation above that.

3. The effect of the *Sandberg et al*. [2014a] cross-calibrated GOES solar proton effective energies on the derived integral fluxes is small at >10 MeV but results in substantial decreases with respect to the current NOAA product at higher energies. The median ratios of the current product to the integral fluxes calculated by using the *Sandberg et al*. [2014a] energies are 1.1, 1.7, 2.1, and 2.9 at >10, >30, >60, and >100 MeV. One consequence of this result is that accurate cross comparisons between current GOES solar proton integral fluxes at >30 MeV and above and any other observations require the use of the *Sandberg et al*. [2014a] effective energies.

Finally, it should be noted that the present work not only validates the *Sandberg et al*. [2014a] cross calibrations between IMP 8 GME and GOES EPS but also demonstrates the good agreement between the GME and STEREO LET and HET observations, using the cross-calibrated GOES 11 data as a calibration transfer.

Appendix A: Description of the Zwickl (1989) Algorithm

The integral flux produced by NOAA SWPC using the algorithm developed by R. Zwickl (unpublished note, 1989, hereafter referred to as Z89) algorithm is a commonly used data set in the fields of space weather and space climate. However, since the algorithm has never been published, the nature of this product is generally not well understood. The purpose of this appendix is to document and interpret the essential mathematics of the Z89 algorithm. It draws on both the unpublished report and its implementation in the C programming language for the processing of the GOES 8–12 data; this appendix is not a mere transcription of the unpublished report.

This algorithm has four primary functions, in the following order: (1) removal of instrumental and galactic cosmic ray backgrounds, (2) correction of EPS proton channel rates for higher-energy contamination, (3) calculation of integral proton flux ($cm^{-2}\,s^{-1}\,sr^{-1}$) above seven energies (1, 5, 10, 30, 50, 60, and 100 MeV), and (4) calculation of differential fluxes ($cm^{-2}\,s^{-1}\,sr^{-1}\,MeV^{-1}$) at six energies (5, 15, 30, 50, 60, and 100 MeV). It operates on 5 min averaged rates, although this is not a limitation of the algorithm.

The algorithm is based on the following special case of the measurement integral. Assuming that a channel has a response with constant G (cm^2 sr) between two energies E_l and E_u and zero elsewhere, and that the proton spectrum being measured follows a power law $j(E) = \alpha E^{-\gamma}$, then the measurement integral simplifies as follows [*Armstrong*, 1976]:

$$C = \int j(E)G(E)dE = \int_{E_l}^{E_u} \alpha E^{-\gamma} G dE = \frac{G\alpha}{-\gamma+1}\left(E_u^{-\gamma+1} - E_l^{-\gamma+1}\right) \tag{A1}$$

(C is used to represent count rate (1/s) in order to avoid confusion with the count ratios R used hereafter.) Therefore, the power law coefficient α is given by

$$\alpha = \frac{C(-\gamma+1)}{G\left(E_u^{-\gamma+1} - E_l^{-\gamma+1}\right)} \tag{A2}$$

and the flux at any energy E_m between E_l and E_u is given by

$$j(E_m) = \frac{C(-\gamma+1)E_m^{-\gamma}}{G\left(E_u^{-\gamma+1} - E_l^{-\gamma+1}\right)} \tag{A3}$$

For a power law differential flux spectrum given by $j(E) = \alpha E^{-\gamma}$, the integral flux between two limits E_1 and E_2 is given by

$$J = \int_{E_1}^{E_2} \alpha E^{-\gamma} dE = \frac{\alpha}{-\gamma+1}\left(E_2^{-\gamma+1} - E_1^{-\gamma+1}\right) \tag{A4}$$

Table A1. Primary (in-Band) Channel Geometrical Factors and Energies Used for GOES 8–15 Processing by Z89 Algorithm

Channel Pi	Geometrical Factor G_i (cm^2 sr)	Geometry-Energy Factor $G\delta E_i$ (cm^2 sr MeV)	$E_{i,l}$ Lower Channel Energy (MeV)	$E_{i,m}$ Mean Channel Energy (MeV)	$E_{i,u}$ Upper Channel Energy (MeV)
P1	0.056[a]	0.202[d]	0.6[a]	2.4[a]	4.2[a]
P2	0.056[a]	0.252[d]	4.2[a]	6.5[a]	8.7[a]
P3	0.056[a]	0.325[d]	8.7[a]	11.6[a]	14.5[a]
P4	0.21[b]	4.64[e]	15[b]	29.5[b]	44[b]
P5	0.36[b]	15.5[c]	39[b]	60.5[b]	82[b]
P6	0.28[b,f]	90.0[e]	84[b]	142[b]	200[b]
P7	0.16[b]	300.0[e]	110[b]	305[b]	500[b]

[a] *Panametrics* [1979, Table 2.3] and discussion on pp. 55–56.
[b] *Panametrics* [1980a, Table 2.5].
[c] *Panametrics* [1980b, Table 1].
[d] *Panametrics* [1981, Table 1.2].
[e] zwork.c processing code, 1994.
[f] Documents have 0.28, code has 0.26.

The responses of the EPS channels were characterized in terms of a primary energy range and multiple secondary (i.e., spurious or contamination) energy ranges, each with its own averaged (flat) geometrical factor [*Panametrics*, 1979, 1980a, 1980b, 1981]. Using this information (Tables A1 and A2), the measurement integral can be separated into multiple energy ranges, each with its own flat geometrical factor; the rates are the sum of those from the lowest (primary) energy range (C^p) and the higher-energy (secondary) ranges are (C^s):

$$C = C^p + C^s = \frac{G\alpha}{-\gamma+1}\left(E_u^{-\gamma+1} - E_l^{-\gamma+1}\right) + \sum_{j=1}^{n} \frac{G_{sj}\alpha_{sj}}{-\gamma_{sj}+1}\left(E_{sj,u}^{-\gamma_{sj}+1} - E_{sj,l}^{-\gamma_{sj}+1}\right) \tag{A5}$$

where the spurious or contamination response of the channel is divided into n segments, each with its geometrical factor G_{sj}, upper and lower energies $E_{sj,u}$ and $E_{sj,l}$, and power law parameters α_{sj} and γ_{sj}. If a single power law (defined by α and γ) is assumed to apply across the energy range of the channel in question, this expression simplifies to

$$C = \frac{\alpha}{-\gamma+1}\left[G\left(E_u^{-\gamma+1} - E_l^{-\gamma+1}\right) + \sum_{j=1}^{n} G_{sj}\left(E_{sj,u}^{-\gamma+1} - E_{sj,l}^{-\gamma+1}\right)\right] \tag{A6}$$

These forms are used in the specific algorithmic steps below.

Table A2. Secondary (Spurious) Geometrical Factors Used for GOES 8–15 Processing by Z89 Algorithm[a]

Channel Pi	Range Index (j)	$E_{sij,l}$ (MeV)	$E_{sij,u}$ (MeV)	G_{sij} (cm^2 sr)
P1	1	50	200	0.02
P2	1	50	125	0.04
	2	125	200	0.007
P3	1	60	125	0.07
	2	125	200	0.014
P4	1	80	115	0.038
	2	115	150	0.25
P5	1	80	110	0.091
	2	110	150	0.57
	3	150	190	0.21
P6	1	80	110	0.15
	2	110	130	0.84
	3	130	200	0.80
	4	200	300	0.26
P7	1	80	110	0.03
	2	110	170	0.15
	3	170	250	1.5
	4	250	500	1.9
	5	500	900	0.56

[a] P1–P3 E_l and E_u and P1 G are from *Panametrics* [1979, Table 3.5], with the upper limit set to 200 MeV. P2–P3 G's have been reduced empirically from their values in Table 3.5. P4–P7 E_l, E_u, and G are from *Panametrics* [1980a, Table 3.4]. None of these characteristics of the P7 channel is used by the Z89 algorithm; the P7 rates are not corrected for the spurious (rear and side entry) responses.

A1. Background Removal

The background to be removed is estimated separately for each channel. Every 5 min a running average of the background is updated by using a 4 h RC filter if the rate is less than some fixed value (Table A3). The updated running average must be greater than 0.0 and less than the previous minimum in order to be recorded as the new minimum background rate. Every 10 days, the background correction is updated if during the previous 10 day period, the number of 5 min records used to update the minimum background

Table A3. Constants Used in Background Removal by Z89 Algorithm

Channel	Upper Limit to Background (s^{-1})	Ratio of Background Correction to Base Rate
P1	0.2	15
P2	0.09	11
P3	0.07	8
P4	0.25	12
P5	0.8	16
P6	1.2	23
P7	2.5	35

rate is equivalent to more than 2 days' worth, and if the difference between the current background correction and the minimum running average rate during the previous 10 day period is greater than 0.4 times or less than −0.2 times the current correction. If so, then the background correction is set to this prior minimum running average, the minimum rate is reset to 0.999, and a quantity called the "base" is calculated by using a channel-dependent fixed ratio with respect to the background correction (Table A3). These ratios were determined from the channel backgrounds and their standard deviations on 07 and 23 March 1989 such that on these days, the base was one fifth the standard deviation of the background levels.

This background correction is subtracted from every rate during the next 10 days. If the corrected rate is less than the base it is set to the base. (As a consequence of this algorithm, jumps are sometimes observed in the corrected fluxes in the absence of an SPE every 10 days, particularly in the channels with larger backgrounds.) The base is also used to determine whether a rate is too low for a dependable determination of a power law exponent.

A2. Contamination Correction

The contamination correction operates on the rates, starting with the highest-energy channel and proceeding to successively lower energies. For channels $1 \le i \le 5$, the power law exponents are calculated as linear functions of the natural logarithm of ratios of rates from adjacent channels:

$$\gamma_{i,i+1} = a_i + b_i \ln\left(R_{i,i+1}\right) \tag{A7}$$

where

$$R_{i,i+1} = \frac{C_i - C_i^s}{C_{i+1} - C_{i+1}^s} \tag{A8}$$

where the rates without the "s" superscript are background-corrected and the rates with the "s" superscript are the secondary rates, estimated as shown below. In calculating R_{67}, the P6 and P7 channel rates are not corrected for contamination; otherwise, the secondary rates are subtracted as in equation (A8) before calculating the ratios. The coefficients a_i and b_i are given in Table A4. For $i = 6$, there are three forms depending on

Table A4. Constants Used by Z89 Algorithm in Calculation of Power Law Exponents and Their Validity Ranges

Exponent	a_i	b_i	$R_{i,i+1}$		$\gamma_{i,i+1}$		
($E^{-\gamma}$)			Min	Max	Min	Max	Default
$\gamma_{1,2}$	0.7	1.3	10^{-3}	0.93	−8	0.6	1.3
	0.65	0.56	0.93	10^{6}	0.6	8	
$\gamma_{2,3}$	0.61	1.86	0.01	0.70	−8	−0.05	1.4
	0.49	1.52	0.70	170	−0.05	8	
$\gamma_{3,4}$	2.85	0.99	10^{-5}	0.12	−8	0.74	1.5
	3.85	1.46	0.12	12	0.74	8[a]	
$\gamma_{4,5}$	1.62	1.55	2×10^{-3}	0.47	−8	0.45	1.7
	1.29	1.11	0.47	500	0.45	8	
$\gamma_{5,6}$	2.19	1.116	10^{-4}	0.83	−8	2	1.9
	2.19	1.17	0.83	130	2	8	
$\gamma_{6,7}$	1.62	0.92	10^{-5}	0.3	−8	0.8	2.0
	See text		0.3	0.4	0.8	1.2	
	2.529 (A)[b]	0.6203 (B)[b]	0.4	6.3	1.2	8	

[a] Z89 has 6 here, but this may be an error since the maximum γ is always 8.
[b] For $R_{67} > 0.4$, the GOES I-M code mistakenly used these coefficients as a and b in equation (A7), instead of as A and B in equation (A9). This has resulted in an underestimate of γ_{67} for $R_{67} > 1$, which exaggerates the effect of counting statistics when the P7 rates are low.

the value of the counts ratio; the ratio ranges are given in Table A4. Equation (A7) is used for the lowest ratio range. For the highest range of ratios,

$$\gamma_{67} = AR_{67}^{B} \tag{A9}$$

The coefficients A and B are given in Table A4. For the intermediate range, γ_{67} is given by the average of the two expressions. If the channel i rate (corrected, apart from that for P6) is less than 5 times the base, then the default $\gamma_{i,i+1}$ for that channel is used (Table A4).

The spurious rates are calculated as follows. The expression for the power law coefficient α_{67} defined by P6 and P7 is a rearrangement of the measurement integral represented by equation (A6). It is a function of the P6 primary and secondary geometrical factors and their associated energies ranging from 80 to 300 MeV (Tables A1 and A2). It is directly proportional to the P6 uncorrected rate, and it is a function of the P7 uncorrected rate through the use of γ_{67}:

$$\alpha_{67} = C_6(\gamma_{67}-1)\left[G_6E_{6,l}^{1-\gamma_{67}} + G_{s6,1}E_{s61,l}^{1-\gamma_{67}} + (G_{s6,2}-G_{s6,1})E_{s62,l}^{1-\gamma_{67}} + (G_{s6,3}-G_{s6,2})E_{s63,l}^{1-\gamma_{67}} + (G_{s6,4}-G_{s6,3}-G_6)E_{s64,l}^{1-\gamma_{67}} - G_{s6,4}E_{s64,u}^{1-\gamma_{67}}\right]^{-1} \tag{A10}$$

Through equation (A10), the P6 and P7 rates affect the corrected rates for P2–P6. In the following expression, the P6 rate correction is defined as the contribution between 200 and 300 MeV, since the in-band P6 energies are defined from 84 to 200 MeV (i.e., the secondary contributions in this latter range are not removed):

$$C_6^s = \frac{\alpha_{67}G_{s64}}{\gamma_{67}-1}\left(E_{s64,l}^{1-\gamma_{67}} - E_{s64,u}^{1-\gamma_{67}}\right) \tag{A11}$$

In the following expression, the P5 rate correction involves all P5 secondary energies, between 80 and 190 MeV. For this energy range, the power law defined by (α_{67}, γ_{67}) is appropriate. The power law coefficient α_{56} is calculated from the corrected P5 rates and the primary characteristics of the P5 channel (39–82 MeV), as well as γ_{56}.

$$C_5^s = \frac{\alpha_{67}}{\gamma_{67}-1}\sum_{j=1}^{3} G_{s5j}\left(E_{s5j,l}^{1-\gamma_{67}} - E_{s5j,u}^{1-\gamma_{67}}\right) \tag{A12}$$

$$\alpha_{56} = \frac{C_5^p(\gamma_{56}-1)}{G_5\left(E_{5,l}^{1-\gamma_{56}} - E_{5,u}^{1-\gamma_{56}}\right)} \tag{A13}$$

The P4 rate correction involves all P4 secondary energies, between 80 and 150 MeV. Therefore, as with P5 and P6, the power law defined by (α_{67}, γ_{67}) is appropriate for this correction:

$$C_4^s = \frac{\alpha_{67}}{\gamma_{67}-1}\sum_{j=1}^{2} G_{s4j}\left(E_{s4j,l}^{1-\gamma_{67}} - E_{s4j,u}^{1-\gamma_{67}}\right) \tag{A14}$$

The P2 and P3 secondary responses range from 50 or 60 MeV, respectively, to 200 MeV, and are characterized in two energy ranges (Table A2). Therefore, both the (α_{56}, γ_{56}) and (α_{67}, γ_{67}) power laws are used in the rate corrections:

$$C_3^s = \frac{\alpha_{56}G_{s31}}{\gamma_{56}-1}\left(E_{s31,l}^{1-\gamma_{56}} - E_{s31,u}^{1-\gamma_{56}}\right) + \frac{\alpha_{67}G_{s32}}{\gamma_{67}-1}\left(E_{s32,l}^{1-\gamma_{67}} - E_{s32,u}^{1-\gamma_{67}}\right) \tag{A15}$$

$$C_2^s = \frac{\alpha_{56}G_{s21}}{\gamma_{56}-1}\left(E_{s21,l}^{1-\gamma_{56}} - E_{s21,u}^{1-\gamma_{56}}\right) + \frac{\alpha_{67}G_{s22}}{\gamma_{67}-1}\left(E_{s22,l}^{1-\gamma_{67}} - E_{s22,u}^{1-\gamma_{67}}\right) \tag{A16}$$

Table A5. Energy Ranges for Power Laws Used in Integral and Differential Flux Calculations by Z89 Algorithm[a]

Power Law	1,2	2,3	3,4	4,5	5,6	6,7
E_1 (MeV)	0.6	4.2	11.6	29.5	60.5	142
E_2 (MeV)	4.2	11.6	29.5	60.5	142	500
Threshold energies within segment (MeV)	1	5, 10	15	30, 50, 60	100	--

[a]These are a mix of lower, mean, and upper primary channel energies from Table A1.

The P1 secondary response has just one energy range starting at 50 MeV; therefore, only the (α_{56}, γ_{56}) power law is used in the correction:

$$C_1^s = \frac{\alpha_{56} G_{s11}}{\gamma_{56} - 1}\left(E_{s11,l}^{1-\gamma_{56}} - E_{s11,u}^{1-\gamma_{56}}\right) \tag{A17}$$

In each case, except P7, the corrected rates are calculated as

$$C_i^p = C_i - C_i^s \tag{A18}$$

If this calculation results in C_i^p less than zero, then it is set to the base rate (Table A3), approximately one fifth the standard deviation of the preevent backgrounds.

A3. Channel Flux Calculation

After the background-corrected rates are corrected for contamination, they are converted to differential directional number flux by dividing by the geometry-energy factors in Table A1:

$$j_i = \frac{C_i^p}{G\delta E_i} \tag{A19}$$

These corrected channel fluxes (protons $cm^{-2}\,sr^{-1}\,s^{-1}\,MeV^{-1}$) are reported as part of the product.

A4. Integral and Differential Flux Calculation

Integral flux is calculated as the sum of integral flux segments that are calculated following equation (A4). The energies for each segment are defined in Table A5. There are six segments corresponding to the six power laws defined by $j_{i,i+1}(E) = \alpha_{i,i+1}\,E^{-\gamma_{i,i+1}}$ $(1 \le i \le 6)$. All the power law exponents $\gamma_{i,i+1}$ and the two power law coefficients α_{56} and α_{67} are defined above. The rest of the power law coefficients $(1 \le i \le 4)$ are calculated similarly to α_{56}:

$$\alpha_{i,i+1} = \frac{C_i^p\left(\gamma_{i,i+1} - 1\right)}{G_i\left(E_{i,l}^{1-\gamma_{i,i+1}} - E_{i,u}^{1-\gamma_{i,i+1}}\right)} \tag{A20}$$

where G_i and $E_{i,l}$ and $E_{i,u}$ are given in Table A1. The integral flux above a given threshold energy E_t is calculated as follows. If E_t lies within energy segment k as indicated in Table A5, then the integral flux above E_t is estimated as

$$J = \frac{\alpha_{k,k+1}}{-\gamma_{k,k+1}+1}\left(E_{k,2}^{-\gamma_{k,k+1}+1} - E_t^{-\gamma_{k,k+1}+1}\right) + \sum_{i=k+1}^{6}\frac{\alpha_{i,i+1}}{-\gamma_{i,i+1}+1}\left(E_{i,2}^{-\gamma_{i,i+1}+1} - E_{i,1}^{-\gamma_{i,i+1}+1}\right) \tag{A21}$$

The upper energy for these integral fluxes is 500 MeV.

The differential flux at E_t is straightforwardly estimated as

$$j(E_t) = \alpha_{k,k+1} E_t^{-\gamma_{k,k+1}} \tag{A22}$$

Both the integral (protons $cm^{-2}\,sr^{-1}\,s^{-1}$) and differential (protons $cm^{-2}\,sr^{-1}\,s^{-1}\,MeV^{-1}$) fluxes are output as part of the product.

Acknowledgments

The work at CIRES was supported in part by the GOES-R program through the Cooperative Agreement with NOAA, and in part by NSF award AGS-1024701 to the University of Colorado. Part of this work was supported by ESA/ESTEC through contract 4000112863/14/NL/HB in the framework of HERMES project. The work at Caltech was supported by NASA under grant NNX11AO75G, and subcontract 00008864 of grant NNX15AG09G. The SEPEM RDS v2.0 is available for download at http://dev.sepem.oma.be/help/SEPEM_RDS_v2-00.zip. The GOES data are available from the National Centers for Environmental Information at http://www.ngdc.noaa.gov/stp/satellite/goes/dataaccess.html. The STEREO data may be requested from the authors. The OMNI data set is available from NASA's Space Physics Data Facility. We thank C. Clark for digitizing all the World Data Center A *Solar-Geophysical Data* and *Upper Atmosphere Geophysics Reports* (http://www.ngdc.noaa.gov/stp/space-weather/online-publications/stp_uag/) and making them readily accessible. The SWPC list of large >10 MeV SPEs is available at ftp://ftp.swpc.noaa.gov/pub/indices/SPE.txt and at http://umbra.nascom.nasa.gov/SEP/. We thank D. Hartley for his density-plot routines and the reviewers for their constructive comments on the original manuscript.

References

Adriani, O., et al. (2016), PAMELA's measurements of geomagnetic cutoff variations during the 14 December 2006 storm, *Space Weather*, *14*, 210–220, doi:10.1002/2016SW001364.

Armstrong, T. P. (1976), *Handbook and Reference Manual for Charged Particle Measurement Experiment Data From Explorer 47 and 50* Preprint JHU/APL 76–02, Johns Hopkins Univ. Appl. Phys. Lab, Laurel, Md.

Armstrong, T. P., C. Brungardt, and J. E. Meyer (1983), Satellite observations of interplanetary and polar cap solar particle fluxes from 1963 to the present, in *Weather and Climate Responses to Solar Variations*, edited by B. M. McCormac, pp. 71–79, Colorado Associated Univ. Press, Boulder.

Bostrom, C. O., D. J. Williams, and J. F. Arens (1968), Solar proton monitoring. In *Solar-Geophysical Data, Descriptive Text,* pp. 61–66, ESSA Research Laboratories, Washington, DC, February 1968. [Available at http://www.ngdc.noaa.gov/stp/space-weather/online-publications/stp_sgd/.]

Crosby, N., et al. (2015), SEPEM: A tool for statistical modeling the solar energetic particle environment, *Space Weather*, *13*, 406–426, doi:10.1002/2013SW001008.

Dichter, B. K., G. E. Galica, J. O. McGarity, S. Tsui, M. J. Golightly, C. Lopate, and J. J. Connell (2015), Specification, design and calibration of the space weather suite of instruments on the NOAA GOES-R program spacecraft, *IEEE Trans. Nucl. Sci.*, *62*, 2776–2783.

Feynman, J., T. P. Armstrong, L. Dao-Gibner, and S. Silverman (1990), New interplanetary proton fluence model, *J. Spacecr.*, *27*, 403–410.
Feynman, J., G. Spitale, J. Wang, and S. Gabriel (1993), Interplanetary proton fluence model: JPL 1991, *J. Geophys. Res.*, *98*, 13,281–13,294, doi:10.1029/92JA02670.
Ginet, G. P., et al. (2013), AE9, AP9 and SPM: New models for specifying the trapped energetic particle and space plasma environment, *Space Sci. Rev.*, *179*, 579–615, doi:10.1007/s11214-013-9964-y.
Green, J. C., T. G. Onsager, T. P. O'Brien, and D. N. Baker (2004), Testing loss mechanisms capable of rapidly depleting relativistic electron flux in the Earth's outer radiation belt, *J. Geophys. Res.*, *109*, A12211, doi:10.1029/2004JA010579.
Grubb, R. N. (1975), The SMS/GOES Space Environment Monitor Subsystem. NOAA Technical Memorandum ERL SEL-42, Space Environment Laboratory, Boulder, Colorado.
Guild, T., P. O'Brien, J. Mazur, and M. Looper (2009), On-orbit inter-calibration of proton observations during solar particle events. *Aerospace Report no. TOR-2007*(*3905*)*-22*.
King, J. H. (1974), Solar proton fluences for 1977–1983 space missions, *J. Spacecr.*, *11*, 401–408, doi:10.2514/3.62088.
King, J. H., and N. Papitashvili (2005), Solar wind spatial scales in and comparisons of hourly Wind and ACE plasma and magnetic field data, *J. Geophys. Res.*, *110*, A02209, doi:10.1029/2004JA010804.
Kohl, J. W. (1968), Solar proton monitoring, *APL Tech. Dig.*, *8*, 2–9.
Kress, B. T., J. V. Rodriguez, J. E. Mazur, and M. Engel (2013), Modeling solar proton access to geostationary spacecraft with geomagnetic cutoffs, *Adv. Space Res.*, *52*, 1939–1948.
Lario, D., A. Aran, R. Gómez-Herrero, N. Dresing, B. Heber, G. C. Ho, R. B. Decker, and E. C. Roelof (2013), Longitudinal and radial dependence of solar energetic particle peak intensities: STEREO, ACE, SOHO, GOES, and MESSENGER observations, *Astrophys. J.*, *767*, 41.
Malitson, H. H., and W. R. Webber (1963), A summary of solar cosmic ray events, in *Solar Proton Manual* NASA TR R-169, edited by F. B. McDonald, pp. 1–17, NASA, Washington, D. C.
Matthiä, D., B. Heber, G. Reitz, L. Sihver, T. Berger, and M. Meier (2009), The ground level event 70 on December 13th, 2006 and related effective doses at aviation altitudes, *Radiat. Prot. Dosim.*, *136*, 304–310, doi:10.1093/rpd/ncp141.
McGuire, R. E., T. T. von Rosenvinge, and F. B. McDonald (1986), The composition of solar energetic particles, *Astrophys. J.*, *301*, 938–961.
Mewaldt, R. A., et al. (2007), Observations of the December 2006 solar energetic particle events with the Low Energy Telescope (LET) on STEREO, *Proc. 30th International Cosmic Ray Conference*, vol. 1 (SH), 107–110.
Mewaldt, R. A., et al. (2008), The Low-Energy Telescope (LET) and SEP central electronics for the STEREO mission, *Space Sci. Rev.*, *136*, 285–362, doi:10.1007/s11214-007-9288-x.
Mewaldt, R. A., R. A. Leske, E. C. Stone, A. F. Barghouty, A. W. Labrador, C. M. S. Cohen, A. C. Cummings, A. J. Davis, T. T. von Rosenvinge, and M. E. Wiedenbeck (2009), STEREO observations of energetic neutral hydrogen atoms during the 2006 December 5 solar flare, *Astrophys. J.*, *693*, L11–L15, doi:10.1088/0004-637X/693/1/L11.
Mewaldt, R. A., C. M. S. Cohen, G. M. Mason, T. T. von Rosenvinge, and A. Vourlidas (2015), A 360° survey of solar energetic particle events and one extreme event *Proceedings of Science*. PoS(ICRC2015)139. 34th International Cosmic Ray Conference, The Hague.
Morley, S. K., J. P. Sullivan, M. G. Henderson, J. B. Blake, and D. N. Baker (2016), The Global Positioning System constellation as a space weather monitor: Comparison of electron measurements with Van Allen Probes data, *Space Weather*, *14*, 76–92, doi:10.1002/2015SW001339.
Mulligan, T., J. B. Blake, and R. A. Mewaldt (2007), Unusual solar energetic proton fluxes at 1 AU within an interplanetary CME, *Proc. 30th International Cosmic Ray Conference*, vol. 1 (SH), 179–182.
O'Brien, T. P. (2009), SEAES-GEO: A spacecraft environmental anomalies expert system for geosynchronous orbit, *Space Weather*, *7*, S09003, doi:10.1029/2009SW000473.
Onsager, T. G., R. Grubb, J. Kunches, L. Matheson, D. Speich, R. Zwickl, and H. Sauer (1996), Operational uses of the GOES energetic particle detectors, in *GOES-8 and Beyond*, *Proc. SPIE*, vol. 2812, edited by E. R. Washwell, pp. 281–290, SPIE - The International Society for Optical Engineering, Bellingham, Washington.
Panametrics (1979), Energetic particle sensor telescope calibration work, PANA-GOESP-CR2. [Available at http://www.ngdc.noaa.gov/stp/satellite/goes/documentation.html.]
Panametrics (1980a), Energetic particle sensor dome calibration work, PANA-GOESP-CR3. [Available at http://www.ngdc.noaa.gov/stp/satellite/goes/documentation.html.]
Panametrics (1980b), Preliminary report on the operation of the EPS S/N 001 and XRS S/N 001 on GOES-D (GOES-4) PANA-SEM-2.
Panametrics (1981), Preliminary report on the operation of the EPS S/N 002 and XRS S/N 002 on GOES-E (GOES-5) PANA-SEM-3.
Richardson, I. G., T. T. von Rosenvinge, H. V. Cane, E. R. Christian, C. M. S. Cohen, A. W. Labrador, R. A. Leske, R. A. Mewaldt, M. E. Wiedenbeck, and E. C. Stone (2014), >25 MeV proton events observed by the high energy telescopes on the STEREO A and B spacecraft and/or at Earth during the first ~ seven years of the STEREO mission, *Sol. Phys.*, *289*, 3059–3107.
Rodriguez, J. V. (2012), Undulations in MeV solar energetic particle fluxes in Earth's magnetosphere associated with substorm magnetic field reconfigurations, *J. Geophys. Res.*, *117*, A06229, doi:10.1029/2012JA017618.
Rodriguez, J. V., T. G. Onsager, and J. E. Mazur (2010), The east-west effect in solar proton flux measurements in geostationary orbit: A new GOES capability, *Geophys. Res. Lett.*, *37*, L07109, doi:10.1029/2010GL042531.
Rodriguez, J. V., J. C. Krosschell, and J. C. Green (2014), Intercalibration of GOES 8–15 solar proton detectors, *Space Weather*, *12*, 92–109, doi:10.1002/2013SW000996.
Sandberg, I., P. Jiggens, D. Heynderickx, and I. A. Daglis (2014a), Cross calibration of NOAA GOES solar proton detectors using corrected NASA IMP-8/GME data, *Geophys. Res. Lett.*, *41*, 4435–4441, doi:10.1002/2014GL060469.
Sandberg, I., J. V. Rodriguez, T. Onsager, P. Jiggens, and I. A. Daglis (2014b), Re-calculating NOAA GOES integral solar proton fluxes paper presented at Eleventh European Space Weather Week, Belgian Solar-Terrestrial Centre of Excellence, Liège, Belgium.
Sauer, H. H., and D. C. Wilkinson (2008), Global mapping of ionospheric HF/VHF radio wave absorption due to solar energetic protons, *Space Weather*, *6*, S12002, doi:10.1029/2008SW000399.
Stassinopoulos, E. G., and J. H. King (1974), Empirical solar proton model for orbiting spacecraft applications, *IEEE Trans. Aeros. Electr. Syst.*, *AES-10*, 442–450.
von Rosenvinge, T. T., et al. (2008), The high energy telescope for STEREO, *Space Sci. Rev.*, *136*, 391–435, doi:10.1007/s11214-007-9300-5.
von Rosenvinge, T. T., I. G. Richardson, D. V. Reames, C. M. S. Cohen, A. C. Cummings, R. A. Leske, R. A. Mewaldt, E. C. Stone, and M. E. Wiedenbeck (2009), The solar energetic particle event of 14 December 2006, *Solar Phys.*, *256*, 443–462, doi:10.1007/s11207-009-9353-6.
Webber, W. R., J. R. Benbrook, J. R. Thomas, A. Hunting, and R. Duncan (1963), An evaluation of the radiation hazard due to solar particle events, The Boeing Company Rep. D2-90469, NTIS AD-805442, 109 pp.